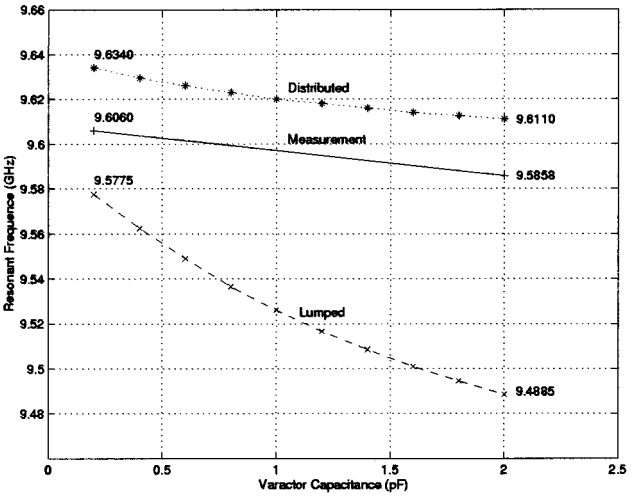

Fig. 3. Tuning range.

V. Conclusion and Further Discussion

The distribution of the coupling between a DR operating in the $\mathrm{TE}_{01\delta}$ mode and microstrip lines has been studied in this paper. Using a finite-element field calculation at the resonant frequency, equivalent multisection circuit parameters were derived. The distributed- and lumped-coupling models are compared with measured results from a test circuit. The distributed model with a predicted tuning range of 23 MHz is in close agreement with the measured range of 20 MHz. The advantage of the distributed model is clear when the range from the lumped model is considered at 89 MHz.

Acknowledgment

The authors would like to thank B. Smith, Philips mmRadiolink U.K. Ltd, Manchester, U.K., and G. Parkinson, Philips mmRadiolink U.K. Ltd, Manchester, U.K., for their generous support.

References

[1] X. Xu and R. Sloan, "Distributed coupling model of the dielectric resonator to microstrip line," *IEEE Microwave Guided Wave Lett.*, vol. 9, pp. 348–350, Sept. 1999.

[2] M. Yousefi and S. K. Chaudhuri, "Dielectric resonator—microstrip interactive circuit analysis and design using integral equation technique," *IEEE Trans. Microwave Theory Tech.*, vol. 43, pp. 1446–1452, July 1995.

[3] K. V. Buer and E.-B. El-Sharawy, "A novel technique for tuning dielectric resonators," *IEEE Trans. Microwave Theory Tech.*, vol. 43, pp. 36–41, Jan. 1995.

[4] D. Kajfez and P. Guillon, *Dielectric Resonators*. Norwood, MA: Artech House, 1986.

[5] Y. Komatsu and Y. Murakami, "Coupling coefficient between microstrip line and dielectric resonator," *IEEE Trans. Microwave Theory Tech.*, vol. MTT-31, pp. 34–40, Jan. 1983.

Rapidly Converging Direct Singular Integral-Equation Techniques in the Analysis of Open Microstrip Lines on Layered Substrates

J. L. Tsalamengas

***Abstract*—In this paper, moment-method-oriented direct singular integral-equation techniques are used for the exact analysis of planar layered microstrip lines. While these techniques retain the simplicity of the conventional method of moments, they optimize them by evaluating all matrix elements via rapidly converging real-axis spectral integrals. The proposed algorithms yield highly accurate results for the dispersion characteristics and for the modal currents both of the fundamental and higher order modes.**

***Index Terms*—Integral equations, layered media, planar transmission lines.**

I. Introduction

Shown in Fig. 1 is the geometry of an open generalized microstrip line. All layers—described by the scalars $(\varepsilon_i,\ \mu_i,\ k_i = \omega\sqrt{\varepsilon_i\mu_i})$—are taken to be linear, homogeneous, and isotropic, whereas the semi-infinite regions $m+1$ and $-n-1$ may be perfect electric conductors (PECs), perfect magnetic conductors (PMCs), or dielectrics. Here, the worst case is considered, where the strip is placed at $(y=0,\ -w \le x \le w,\ -\infty < z < +\infty)$ right on the interface between two adjacent layers. It is known [1], [2] that, in this (worst) case, several exponentially decaying factors, which ensure convergence of the conventional spectral Green's dyads, disappear, leaving us with slowly converging spectral integrals. Proper handling of these integrals will be carried out most efficiently in Section III.

In connection with this structure, the three-dimensional (3-D) excitation problem for an arbitrarily polarized obliquely incident plane wave has been treated in [3]. Here, we solve the spectral (propagation) problem. Since the analysis is the same for both problems, only a brief outline will be given here, referring to [3] for details. The corresponding generalized microslot-line problem has been recently treated in [4] along parallel lines.

The analysis begins with the system of integral equations (rather inconvenient) derived in the context of conventional method of moments (MoM) by the immittance approach. The next crucial step is to recast this system into a 2×2 system of first-kind singular integral/integrodifferential equations (SIE/SIDE). Most advantageously, the new kernels consist of: 1) several closed-form (Hankel) singular terms and 2) rapidly converging real-axis spectral integrals. With the help of some basic algorithms developed in [5], the solution of the final SIE/SIDE leads to matrix elements, the representations of which converge very rapidly.

II. Analysis

Assuming propagation in the $-z$-direction and following the immittance approach, the surface current density on the strip $\overline{J} = [J_x(x)\hat{x} + J_z(x)\hat{z}]e^{j(\omega t+\beta z)}$ is found to satisfy the system of integral equations

$$\Re(Z_1,\ Z_2;x) = 0 \quad \Re(Z_2,\ Z_3;x) = 0 \ \ (|x| \le w) \tag{1}$$

Manuscript received September 20, 1999.

The author is with the Department of Electrical and Computer Engineering, National Technical University of Athens, GR-157 73 Athens, Greece (e-mail: itsal@central.ntua.gr).

Publisher Item Identifier S 0018-9480(01)01694-5.

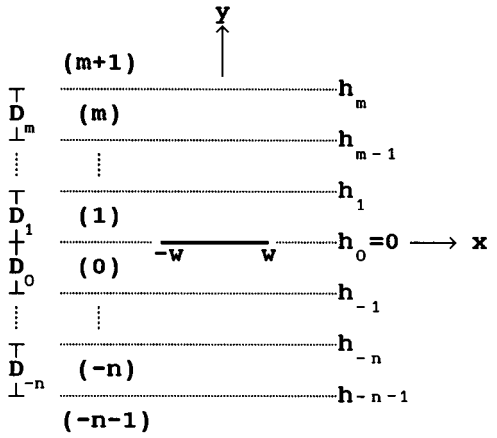

Fig. 1. Geometry of the problem.

where $\Re$ is the shorthand symbol for

$$\Re(Z_i,\, Z_j; x) \equiv \frac{1}{2\pi}\int_{-w}^{w} dx' \int_{-\infty}^{\infty} e^{-ju(x-x')} \cdot\Big[Z_i(u)J_x(x') + Z_j(u)J_z(x')\Big]\, du. \quad (2)$$

Here,

$$Z_j(u) = Z_j(u; \Psi^e,\, \Psi^h)$$

$(j = 1,\, 2,\, 3)$ are given by [3, eq. (7)] in terms of the quantities

$$\Psi^e = Y^e(0+) - Y^e(0-) \quad \Psi^h = Y^h(0+) - Y^h(0-) \quad (3)$$

where $Y^q(y) \equiv Y^q(u; y)$ $(q \equiv e,\, h)$ are the admittances of the LSE^y and LSM^y waves supported by the layered dielectric medium in the absence of the strip. $Y^q(0+)$ and $Y^q(0-)$ may be recursively evaluated, as explained in [3, App. A].

A. Discretization of (1) by Conventional MoM

We set $x = wt,\, x' = wt'$ $(-1 \le t,\, t' \le 1)$ and expand

$$J_z\Big[x(t)\Big] = F_z(t)\Big/\sqrt{1-t^2},\; F_z(t) = \sum_{N=0}^{\infty} a_N T_N(t) \quad (4a)$$

$$J_x\Big[x(t)\Big] = F_x(t)\sqrt{1-t^2},\; F_x(t) = \sum_{N=0}^{\infty} b_N U_N(t) \quad (4b)$$

where T_N and U_N are the Chebyshev polynomials and a_N and b_N are expansion constants. Inserting (4a) and (4b) into the first and second equations of (1), multiplying the first and second equations of (1), respectively, by $\sqrt{1-t^2}U_M(t)$ and by $T_M(t)/\sqrt{1-t^2}$ $(M = 0,\, 1,\, 2,\, \ldots)$, and integrating from $t = -1$ to $t = 1$ yields the infinite linear algebraic system

$$\sum_{N=0}^{\infty}\begin{pmatrix} K^{zz}_{MN} & K^{zx}_{MN} \\ K^{xz}_{MN} & K^{xx}_{MN}\end{pmatrix}\begin{pmatrix} a_N \\ b_N\end{pmatrix} = \begin{pmatrix} 0 \\ 0\end{pmatrix}, \qquad M = 0, 1, 2, \ldots, \infty. \quad (5)$$

Here,

$$\begin{aligned} K^{xx}_{MN} &= I^{11}_{MN}(Z_1)d^{+}_{MN} \\ K^{xz}_{MN} &= -K^{zx}_{NM} \\ &= I^{10}_{MN}(Z_2)\, d^{-}_{MN} \\ K^{zz}_{MN} &= I^{00}_{MN}(Z_3)\, d^{+}_{MN} \end{aligned} \quad (6)$$

$$d^{\pm}_{MN} = \Big[1 \pm (-1)^{M+N}\Big]\Big/2 \quad (7)$$

where $I^{mn}_{MN}(Z_j)$ $(m,\, n = 0,\, 1; j = 1,\, 2,\, 3)$ are the following spectral integrals

$$I^{mn}_{MN}(Z_j) = -\pi w(-1)^M j^{M+N}(M+1)^m(N+1)^n \cdot\int_0^{\infty} Z_j(u)\frac{J_{M+m}(wu)}{(wu)^m}\,\frac{J_{N+n}(wu)}{(wu)^n}\, du \quad (8)$$

with J_n denoting the Bessel function of order n. The dispersion equation of the problem results by setting the determinant of the system (5) to zero.

It may be verified that $Z_j(u)$ vary as $|u|^{2-j}$ $(j = 1,\, 2,\, 3)$ when $u \to \pm\infty$. Therefore, the integrals $I^{mn}_{MN}(Z_j)$ converge slowly, as u^{-2}. As a consequence, it is difficult to obtain a high accuracy on the basis of (5) and (6) for the modal electric currents and for the propagation constant. This is true, in particular, for high-order modes, necessary when studying, for example, microstrip discontinuities. To overcome these difficulties, a singularity extraction procedure is applied in the following section. An alternative efficient spectral-domain technique has been developed in [6].

III. Singularity Extraction

To recast (1) into a convenient form, we use the decompositions [3]

$$\frac{1}{\Psi^q(u)} = \frac{1}{y^q_1 + y^q_0} + P^q(u), \qquad q \equiv e,\, h$$

$$Z_j(u) = \zeta_j(u) + Z^{(j)}(u), \qquad j = 1,\, 2,\, 3 \quad (9)$$

where

$$\zeta_j(u) = Z_j\Big(u; y^e_1 + y^e_0,\, y^h_1 + y^h_0\Big)$$

$$Z^{(j)}(u) = Z_j\left(u; \frac{1}{P^e},\, \frac{1}{P^h}\right) \quad (10)$$

$$\begin{aligned} y^e_i &= -j\omega\varepsilon_i/\gamma_i \\ y^h_i &= -j\gamma_i/(\omega\mu_i) \\ \gamma_i &= (u^2 - \kappa_i^2)^{1/2} \\ \kappa_i^2 &\equiv k_i^2 - \beta^2 \quad \Big(-\frac{\pi}{2} < \arg(\gamma_{-n-1}) \le \frac{\pi}{2}, \\ &\qquad -\frac{\pi}{2} < \arg(\gamma_{m+1}) \le \frac{\pi}{2}\Big). \end{aligned} \quad (11)$$

It may be verified that $P^q(u)$ and $Z^{(j)}(u)$ decay very strongly (exponentially) as $u \to \pm\infty$, whereas $\zeta_j(u)$ continue to vary as $|u|^{2-j}$, which is rather inconvenient. Proper handling of the inverse Fourier integrals $\int_{-\infty}^{\infty} \zeta_j(u)e^{-ju(x-x')}\, du$, as described in [3], leads to the following system of SIE/SIDE:

$$\begin{aligned} \Re(R_1,\, R_2; x) &+ \left(k_A^2\frac{d^2}{dx^2} + k_C^2\right)\Im_x^{(1)}(x) \\ &+ \left(k_B^2\frac{d^2}{dx^2} + k_D^2\right)\Im_x^{(2)}(x) \\ &+ j\beta\frac{d}{dx}\Big[k_A^2\Im_x^{(1)}(x) + k_B^2\Im_x^{(2)}(x)\Big] = 0 \end{aligned} \quad (12a)$$

$$\begin{aligned} \Re(R_2,\, R_3; x) &+ j\beta\frac{d}{dx}\Big[k_A^2\Im_x^{(1)}(x) + k_B^2\Im_x^{(2)}(x)\Big] \\ &- T_A\Im_x^{(1)}(x) - T_B\Im_x^{(2)}(x) = 0 \end{aligned} \quad (12b)$$

$(|x| \le w)$. Here, the notation

$$\Im_p^{(1)}(x) \equiv \int_{-w}^{w} J_p(x')H_0^{(2)}(\kappa_1|x-x'|)\, dx'$$

$$\Im_p^{(2)}(x) \equiv \int_{-w}^{w} J_p(x')K(|x-x'|)\, dx' \qquad p \equiv x,\, z \quad (13)$$

has been used with

$$K\left(|x-x'|\right) = \frac{1}{\kappa_1^2-\kappa_0^2}\sum_{s=0}^{1}(-1)^s\kappa_s^2 \cdot\left[H_0^{(2)}\left(\kappa_s|x-x'|\right)+H_2^{(2)}\left(\kappa_s|x-x'|\right)\right] \tag{14}$$

($H_0^{(2)}$ and $H_2^{(2)}$ being Hankel functions). The quantities R_j ($j=1,\,2,\,3$) (rapidly converging functions of the spectral variable u), $k_A^2,\,k_B^2,\,k_C^2,\,k_D^2,\,T_A$, and T_B are defined in [3, App. B].

A. Discretization of (14) using DSIET

The discretization of (14) will be based on two of the direct singular integral-equation techniques (DSIETs) developed in [4] as follows.

Method A: This method, outlined in [4, Sec. III], yields for the matrix elements in (5) the expressions

$$K_{MN}^{xx} = \left\{-I_{MN}^{11}(R_1)+\frac{1}{w}\cdot\left[k_A^2 D_{MN}^{(1)}\left(\frac{k_C^2}{k_A^2},\,\kappa_1 w\right)+k_B^2 D_{MN}^{(2)}\left(\frac{k_D^2}{k_B^2},\,\kappa_1 w,\,\kappa_{-1}w\right)\right]\right\} d_{MN}^{+} \tag{15a}$$

$$K_{MN}^{xz} = -K_{NM}^{zx} = \left\{-I_{MN}^{10}(R_2)+j\beta\left[k_A^2 C_{MN}^{(1)}(\kappa_1 w)+k_B^2 C_{MN}^{(2)}(\kappa_1 w,\,\kappa_{-1}w)\right]\right\} d_{MN}^{-} \tag{15b}$$

$$K_{MN}^{zz} = \left\{-I_{MN}^{00}(R_3)-w\left[T_A A_{MN}^{(1)}(\kappa_1 w)+T_B A_{MN}^{(2)}\cdot(\kappa_1 w,\,\kappa_{-1}w)\right]\right\} d_{MN}^{+} \tag{15c}$$

where F_{MN}^{q} ($F\equiv A,\,B,\,C,\,D;\,q\equiv 1,\,2$) are given in a computationally efficient form in [4]. The spectral integrals $I_{MN}^{mn}(R_j)$, which have to be evaluated numerically, converge as u^{-6}, i.e., very rapidly. Finally, let us assume that each of the series in (4a) and (4b) is truncated at $N=N_r$. By embodying several symmetry relations, as explained in [4], it may then be shown that $(N_r+1)\times(N_r+2)$ integrations suffice in order to fill up all the $4(N_r+1)^2$ matrix elements. The above features considerably add to the efficiency of the algorithm.

Method B: This method, outlined in [4, Sec. V], ends up with the linear algebraic system of

$$\sum_{n=1}^{L}\begin{pmatrix}\tilde{R}_{mn}^{zz} & \tilde{R}_{mn}^{zx}\\ \tilde{R}_{mn}^{xz} & \tilde{R}_{mn}^{xx}\end{pmatrix}\begin{pmatrix}c_n\\ d_n\end{pmatrix}=\begin{pmatrix}0\\ 0\end{pmatrix},\qquad n=1,\,2,\ldots,L \tag{16}$$

with unknowns the quantities

$$c_n \equiv F_z(t_n)$$
$$d_n \equiv F_x(\hat{t}_n),\qquad n=1,\,2,\,\ldots,\,L \tag{17}$$

$$t_n = \cos\frac{(2n-1)\pi}{2L}$$
$$\hat{t}_n = \cos\frac{n\pi}{L+1}. \tag{18}$$

The integer L, determining the matrix size $2L\times 2L$, is as large as needed to ensure convergence of the algorithm. The matrix elements $\tilde{R}_{mn}^{zz}$ in (16), as given in [3, eq. (28)], involve: 1) the spectral integrals $J^q(t,\,\tau;R_j)$ ($q\equiv a,\,b;j=1,\,2,\,3$), which are defined in [3, eq. (20)] and converge uniformly, as $1/|u|^{3+j}$ and 2) the quantities $\tilde{F}_{mn}^{(q)}$ ($F\equiv A,B,\,C,\,D;q=1,\,2$) of [4], which are given either in closed form or in terms of simple single series. These important features considerably enhance the efficiency of algorithm B.

In terms of $\{c_n,\,d_n\}$, the modal electric current density on the strip may be found via [3, eq. (21)].

IV. Numerical Results and Validation of the Algorithms

To validate the proposed algorithms (methods A and B), exhaustive comparisons of their corresponding results have been carried out along with comparisons with results available from [7]–[12].

Table I concerns an open microstrip line (like that depicted in the insets of Fig. 2 (for $d_0\to\infty$) or Fig. 3) of relative dielectric constant $\varepsilon_r=8$. Highly accurate results are shown for the effective dielectric constant $\varepsilon_{\text{eff}}=(\beta/k_0)^2$, as computed by both method A (for several truncation sizes, $N=1-6$) and method B. Here, both a narrow strip ($2w/d=0.1$) and a wide one ($2w/d=1.0$) are considered for several values of d/λ_0 ($d=$ substrate thickness, $\lambda_0=$ free-space wavelength). As seen, the convergence of method A is extremely rapid and stable. In the case $2w/d=0.1$, the results obtained by method B are in exact agreement with those of method A. The agreement between these two independent methods is excellent for the case $2w/d=1$ as well. In both cases, results reported in [7]–[10] are also included for the sake of comparison. Inspection reveals that, for narrow strips, our results are in excellent agreement with those of [7] and [8]. In contrast, for wide strips, our results are in excellent agreement with those of [9].

Fig. 2 shows ε_{eff} of a shielded microstrip line for several parameter values. These results are indistinguishable from [11, Fig. 4(a)]. The results of [11, Fig. 3(a)] have been also reproduced exactly using both our methods (not shown).

The proposed algorithms can be most efficiently used to study higher order modes as well. This is exemplified in Table II, where β/k_0 is shown for the three consecutive modes of an open microstrip line (see the inset of Fig. 3) with parameters $2w=3$ mm, $d=0.635$ mm, and $\varepsilon_r=9.8$. Analogous results pertaining to this same structure have been most recently published in [12] based on the mixed-potential integral equation combined with complex image theory. As seen, the results of our methods A and B are in excellent agreement to each other. These results are also in very good agreement with those of [12] for the first and second modes. For the third mode, in contrast, our results deviate (up to 4.9%) from those of [12]. To resolve the dilemma posed by these discrepancies, we turn to an idea presented in [13, Sec. 4.9] and consider the microstrip line, which results after imposing perfectly conducting electric sidewalls at $x=\pm A$. This new (modified) structure can be independently studied using Fourier series (thus avoiding any numerical integration) with extremely high accuracy by extending the powerful techniques recently presented in [14]. For A large enough (e.g., $A>15\,\max(d,\,w)$ as suggested in [13]), the sidewalls have negligible effect on the characteristics of the microstrip line. As a matter of fact, the results for the modified microstrip line (for $A=30d$, using six basis functions for each of J_x and J_z)—shown also in Table II (rows labeled "MS")—are found to coincide (to within six significant decimals) with those of our method A. This coincidence of results clearly demonstrates the efficiency and high accuracy of the proposed algorithms in studying higher order modes.

The algorithms proposed here may be also used to obtain the modal current densities on the strip with high accuracy. To this end, one has to solve the homogeneous systems of (5) (method A) or (16) (method B)

TABLE I
EFFECTIVE DIELECTRIC CONSTANT OF AN OPEN MICROSTRIP LINE, AS OBTAINED BY METHODS A AND B, AND COMPARISON WITH [7]–[10]

		2w/d=0.1						
d/λ_0		0.05	0.1	0.2	0.3	0.4	0.7	1.0
Method								
A	N=1	5.270382	5.765638	6.799307	7.376902	7.633300	7.875877	7.938582
	2	5.270382	5.765641	6.799319	7.376913	7.633309	7.875881	7.938586
	3	5.270382	5.765641	6.799317	7.376911	7.633307	7.875880	7.938585
B		5.270382	5.765641	6.799317	7.376911	7.633307	7.875880	7.938585
[7]		5.270	5.765	6.799	7.367	7.633	7.876	7.939
[8]		5.270	5.765	6.799	7.376	7.633	7.876	7.939
[9]		5.384	5.765	6.791	7.365	7.617	7.872	7.938
		2w/d=1						
d/λ_0		0.05	0.1	0.2	0.3	0.4	0.7	1.0
Method								
A	N=3	6.124938	6.752812	7.393362	7.654112	7.778974	7.914988	7.955581
	4	6.124938	6.752813	7.393365	7.654122	7.778974	7.915222	7.955459
	5	6.124938	6.752812	7.393357	7.654093	7.778939	7.914934	7.955531
	6	6.124938	6.752812	7.393357	7.654093	7.778939	7.914934	7.955533
B		6.124938	6.752811	7.393351	7.654083	7.778927	7.914930	7.955521
[7]		6.124	6.742	7.361	7.620	7.747	7.898	7.945
[8]		6.1272	6.7576	7.3996	7.6591	7.7826	7.9164	7.9562
[9]		6.130	6.753	7.393	7.654	7.778	7.914	7.948
[10]		6.1316	6.7572	-	7.6551	-	7.9151	7.9556

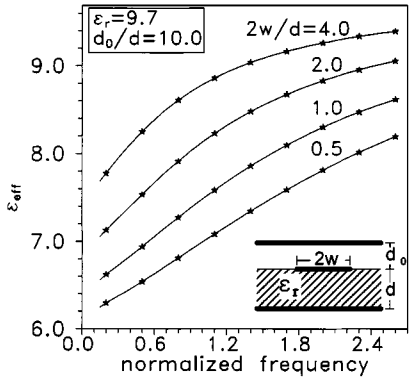

Fig. 2. Effective dielectric constant versus normalized frequency for a shielded microstrip line (———: this paper , ***: [11]).

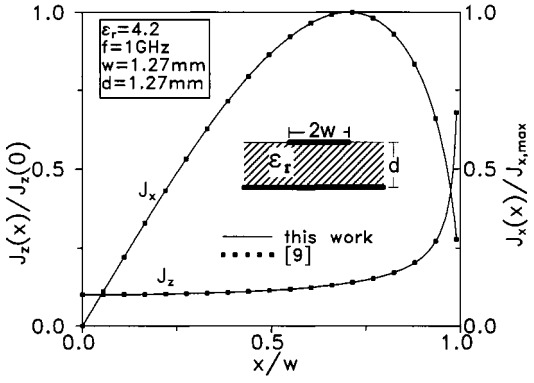

Fig. 3. Modal currents of the first mode of an open microstrip line.

on the basis of the singular-value decomposition method. Typical results are plotted in Fig. 3 in connection with the first mode of the open microstrip line shown in the inset. These results are indistinguishable from those of [9] providing a further validity test of the developed numerical code.

TABLE II
β/k_0 FOR THE FUNDAMENTAL AND FIRST TWO HIGHER MODES OF AN OPEN MICROSTRIP LINE WHEN $2w = 3$ mm, $d = 0.635$ mm, AND $\varepsilon_r = 9.8$

fr (GHz)	Method		1st Mode	2nd Mode	3rd Mode
30	A	5	3.0272114	2.5799588	1.4045527
		6	3.0272111	2.5799588	1.4044689
		7	3.0272111	2.5799588	1.4044702
	B		3.02720	2.58001	1.40447
	MS		3.0272112	2.579959	1.404470
	[12]		3.026	2.579	1.334
35	A	5	3.0433918	2.6972272	1.8849176
		6	3.0433914	2.6972271	1.8847276
		7	3.0433914	2.6972272	1.8847296
	B		3.04337	2.69728	1.88472
	MS		3.043391	2.697227	1.884729
	[12		3.042	2.696	1.818
40	A	5	3.0561774	2.7782170	2.1736055
		6	3.0561770	2.7782173	2.1732900
		7	3.0561770	2.7782173	2.1732994
	B		3.05615	2.77828	2.17329
	MS		3.056177	2.778217	2.173299
	[12]		3.054	2.778	2.110
45	A	5	3.0664269	2.8372460	2.3657118
		6	3.0664263	2.8372464	2.3652685
		7	3.0664263	2.8372463	2.3652706
	B		3.06640	2.83732	2.36526
	MS		3.066426	2.837246	2.365270
	[12]		3.064	2.836	2.306
50	A	5	3.0747513	2.8819587	2.5021460
		6	3.0747504	2.8819591	2.5015458
		7	3.0747504	2.8819591	2.5015481
	B		3.07472	2.88203	2.50153
	MS		3.074750	2.881959	2.501548
	[12]		3.071	2.881	2.445

MS: Modified structure (microstripline with side walls)

Concerning the third (higher order) mode of Table II for $f = 30$ GHz ($\beta/k_0 = 1.404470$), Fig. 4 shows $Z_0 J_z$ (dotted line) and $Z_0 J_x$ (solid line) versus x/w ($Z_0 = \sqrt{\mu_0/\varepsilon_0}$). These curves have

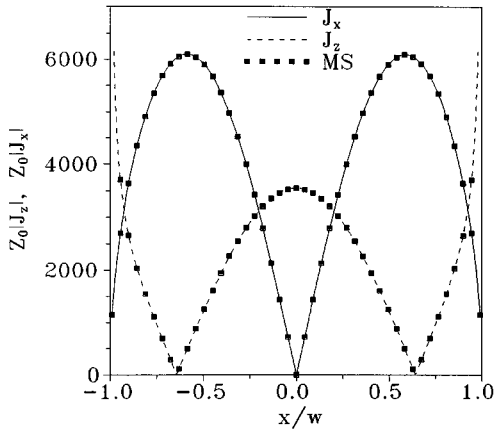

Fig. 4. Modal currents of the third mode of Table II for $f = 30$ GHz ($\beta/k_0 = 1.404470$).

been derived by using method A and reproduced exactly by method B as well. As a further test of the correctness of these results, we also derived analogous curves pertaining to the modified microstrip line (labeled "MS"), with conducting sidewalls, referred to earlier in connection with Table II. As a matter of fact, the curves pertaining to this modified structure were found to be indistinguishable from those obtained earlier by methods A and B.

V. Conclusion

Two independent DSIETs have been used for the exact full-wave analysis of layered microstrip lines. The proposed algorithms combine the simplicity of conventional MoMs with extremely high accuracy both for the propagation constants and modal currents on the strip. In filling up the matrix elements, only rapidly converging real-axis spectral integrals are encountered.

References

[1] N. G. Alexopoulos, "Integrated circuit structures on anisotropic substrates," *IEEE Trans. Microwave Theory Tech.*, vol. MTT-33, pp. 847–881, Oct. 1985.

[2] T. Itoh, *Numerical Techniques for Microwave and Millimeter-Wave Passive Structures*. New York: Wiley, 1989.

[3] J. L. Tsalamengas, "Scattering of arbitrarily polarized plane waves obliquely incident on infinite slots or strips in a planar stratified medium," *IEEE Trans. Antennas Propagat.*, vol. 46, pp. 1634–1640, Nov. 1998.

[4] ——, "Exponentially converging direct singular integral equation methods in the analysis of microslot-lines on layered substrates," *IEEE Trans. Microwave Theory Tech.*, vol. 47, pp. 2031–2034, Oct. 1999.

[5] ——, "Direct singular integral equation methods in scattering and propagation in strip- or slot-loaded structures," *IEEE Trans. Antennas Propagat.*, vol. 46, pp. 1560–1570, Oct. 1998.

[6] F. Mesa, R. Marques, and M. Horno, "An efficient numerical spectral domain method to analyze a large class of nonreciprocal planar transmission lines," *IEEE Trans. Microwave Theory Tech.*, vol. 40, pp. 1630–1641, Aug. 1992.

[7] M. Kobayashi and F. Ando, "Dispersion characteristics of open microstrip lines," *IEEE Trans. Microwave Theory Tech.*, vol. MTT-35, pp. 101–105, Feb. 1987.

[8] M. Kobayashi and T. Iijima, "Frequency-dependent characteristics of current distributions on microstrip lines," *IEEE Trans. Microwave Theory Tech.*, vol. 37, pp. 799–801, Apr. 1989.

[9] C. Shih, R.-B. Wu, S.-K. Jeng, and C. H. Chen, "A full-wave analysis of microstrip lines by variational conformal mapping technique," *IEEE Trans. Microwave Theory Tech.*, vol. 36, pp. 576–581, Mar. 1988.

[10] S.-O. Park and C. A. Balanis, "Dispersion characteristics of open microstrip lines using closed-form asymptotic extraction," *IEEE Trans. Microwave Theory Tech.*, vol. 45, pp. 458–460, Mar. 1997.

[11] A.-M. A. El-Sherbiny, "Exact analysis of shielded microstrip lines and bilateral finlines," *IEEE Trans. Microwave Theory Tech.*, vol. MTT- 29, pp. 669–675, July 1981.

[12] J. Bernal, F. Medina, R. R. Boix, and M. Horno, "Fast full-wave analysis of multistrip transmission lines based on MPIE and complex image theory," *IEEE Trans. Microwave Theory Tech.*, vol. 48, pp. 445–452, Mar. 2000.

[13] R. E. Collin, *Field Theory of Guided Waves*. New York: IEEE Press, 1991.

[14] J. L. Tsalamengas, "Rapidly converging spectral-domain analysis of shielded layered finlines," *IEEE Trans. Microwave Theory Tech.*, vol. 47, pp. 805–810, June 1999.

MIM Shunt-Capacitor Model Using Black Boxes of EM-Simulated Critical Parts

Gregor Gerhard and Stefan Koch

***Abstract*—A new model for metal–insulator–metal shunt capacitors is introduced in this paper. The main difference between the new model and known models is that critical parts of the capacitor's geometry are represented by black boxes. These boxes contain S-parameter files generated with an electromagnetic field solver. The capacitor parts, which depend on the capacitance value, are represented by microstrip and lumped elements. The new model combines the advantages of field simulations with those of lumped- or microstrip-based models. It can easily be used in circuit simulators utilizing their features for design development such as optimizations. The model is compared with two shunt capacitors on microwave monolithic integrated circuits to show the excellent fit.**

***Index Terms*—Capacitor, EM simulation, MIM, model.**

I. Introduction

Metal–insulator–metal (MIM) shunt capacitors are key elements in many microwave and millimeter-wave monolithic integrated circuits (MMICs). DC blocks, matching sections, and biasing circuitry widely utilize this component because of its small space requirement. An accurate model of the structure is, therefore, crucial for any MMIC design. Many monolithic foundries have developed their own proprietary models by means of parameter-extraction methods from experimental data. Other approaches, closer to the physical structure of the MIM capacitor, have been previously presented for series MIM capacitors, resulting in a distributed [1] or lumped [2] equivalent model. Other models calculate the equivalent-circuit parameters with complex formulas based on S-parameter matrices to consider several layout cases [3]. More universal models, as in [4], naturally show less accuracy than

Manuscript received October 4, 1999.

The authors are with Marconi Communications GmbH, D-71522 Backnang, Germany.

Publisher Item Identifier S 0018-9480(01)01695-7.